Role of Magnetic Materials in a Novel Electrical Motogenerator for the 'More Electric Aircraft'

Published paper @DOI: 10.1109/TMAG.2013.2284937

Role of Magnetic Materials in a Novel Electrical Motogenerator for the "More Electric Aircraft"

O. Bottauscio*, G.Serra**, M. Zucca*, M. Chiampi***

* Electromagnetics Division, Istituto Nazionale di Ricerca Metrologica, INRIM, Strada delle Cacce 91, 10135, Torino, Italy
** Dip. Ing. dell'Energia Elettrica e dell'Informazione, Università di Bologna, Viale Risorgimento 2, 40126 Bologna, Italy
*** Dip. Energia, Politecnico di Torino, Corso Duca degli Abruzzi 24, 10129 Torino, Italy

The more electric engine concept considers the electric motor-generators included inside the aircraft reactor. Due to the environment characteristics the problem of reducing the losses in these machines becomes crucial. For such a purpose, this paper focuses on the magnetic losses, analyzing a small (10 kW) 12-phase induction motor-generator prototype through a validated numerical approach. Authors demonstrate that, with respect to the more traditional Fe-Si rotor core, the use of a Fe-Co alloy in the rotor reduces the total losses of up to 1%, and specifically the iron losses up to 7%, while increasing the generated electrical power up to 3%.

***Index Terms* – Electromagnetic modeling, Fault tolerant systems, Induction motors, Magnetic losses**

I. Introduction

In avionics the term "More Electric Aircraft", indicates the trend of replacing in total or partially the centralized mechanical power systems with the electrical ones. More specifically, the so-called More Electric Engine (MEE) conception aims at developing electrical machines integrated inside the main gas turbine to generate electrical power for the aircraft, start the engine and guarantee generation in case problems arise during the flight [1]. Such devices can be defined, in general, as electrical motogenerators although its use as a motor is only required during the starting operation. They must operate in a wide speed range with high efficiency to exploit the energy of the reactor at best. Moreover, the high temperature of the engine ambient significantly limits the dissipation of the heat generated inside the machine, so requiring any action to reduce the losses.

Candidate machines for the embedded starter/generator application are induction and permanent magnet synchronous machines. The high speed and relatively low demanded torque, as well as the "natural" flux weakening capability required by the constant power generation, make induction machines well suited for the application. Furthermore, the mechanical and thermal limits of the magnets could be not compatible with the temperature constrains of the application. Finally, permanent magnet machines are intrinsically less fault tolerant [2, 3], due to the unavoidable back emf induced by the rotating magnets.

Multi-phase induction machines show advantages with respect to their three-phase counterparts, because load power can be split among multiple phases, leading to power switching devices with reduced rating. Moreover, a high phase number of the drive can be exploited in different ways, such as increasing the torque density, developing multi-motor drives, and improving the fault tolerant capability [4]. Multiple three-phase machines have been utilized in some applications [5,6].

In this paper the iron losses in a MEE motogenerator have been analyzed making use of a validated Finite Element (FEM) modeling approach [7,8]. In particular two machine configurations, with laminated rotor cores made of Fe-Si and Fe-Co, are compared in terms of energy losses versus speed and versus the distribution inside the machine. The results evidence a significant advantage in the use of the Fe-Co rotor.

II. Features of the Considered Motogenerator

The machine under investigation is a 12-phases, four poles small prototype having 10 kW rated power and 80 mm axial length. The nominal air-gap is 0.7 mm, whilst other parameters are given in Table I. The motogenerator is expected to cover a wide speed range, from 6000 rpm up to 15000 rpm. For this reason, the supply phase voltage is envisaged to linearly increase with frequency up to ~143V at 270 Hz; the last value is kept constant for further frequency increase. In this study the geometry of the whole device is fixed and employs thin laminations (~0.2 mm thick) in the magnetic core. The stator is always composed of a Fe-Si alloy by Cogent, while two rotors have been considered: one made of the same Fe-Si alloy and the other one made of Fe-Co alloy by Vacuumschmelze.

The analysis of the device has been made through a well validated finite element code [7, 8], briefly described in Sect. III. Anyway, preliminary tests developed in comparison with a commercial code (Flux™) have shown a satisfactory agreement in the evaluation of the flux density inside the machine and of the winding currents (Fig. 1b).

III. Modeling Approach to Magnetic Losses

A. *Finite Element analysis*

The field problem is formulated in time-domain in terms of magnetic vector potential, handling the magnetic nonlinearity

TABLE I
DEVICE PARAMETERS

Parameter	Stator	Rotor
Number of slots	48	40
Ext. diameter [mm]	200.0	108.6
Int. diameter [mm]	110.0	40.0
Conductors per slot	17	1

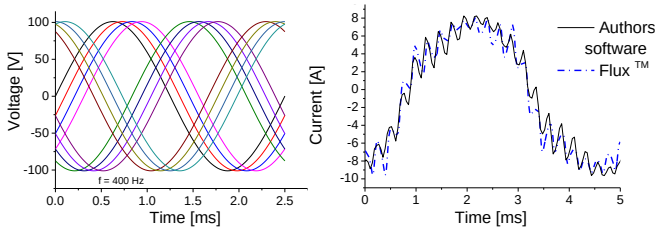

Fig. 1 - a) Supply voltages at 400 Hz, b) Computed currents at synchronous speed at 200 Hz. Comparison between the current waveforms obtained by the Authors code and the ones obtained with Flux™ commercial code.

through the fixed point (FP) technique. The FEM analysis involves both the coupled electric circuits (voltage-driven problem) and the mechanical actions (i.e. the motion of the rotor) by adopting a sliding mesh technique in the air-gap region. Details about model implementations can be found in [7]. FEM simulations are developed including the non-linear magnetic characteristic, but disregarding hysteresis and computing the magnetic losses a-posteriori. Such a simplifying assumption does not affect the result accuracy [8].

B. Identification of the material properties

The magnetic properties of the electrical steels are determined starting from Epstein measurements in the frequency range up to 10 kHz, differently from [9], where hysteresis loops are directly measured on the machine core.

Despite the small thickness, laminations approach the skin effect regime that can be modeled with different degrees of accuracy [10]. In our case, flux penetration into the lamination depth is studied by coupling a 1-D laminated model [11] with the dynamic Preisach hysteresis model (DPM) proposed by Bertotti [12] (laminated-Preisach model). Congruency properties of Preisach model are corrected by a first order moving term (k_1) in the effective field. By adopting a self-consistent procedure, the dynamic constant k_d of DPM ($dM/dt = k_d\left(H-\alpha\right)$) and the moving term k_1 are evaluated for Fe-Si and Fe-Co steels (see Table II). Dynamic loop reconstructions are shown in Fig. 2.

C. Magnetic loss model in the lamination

Even in presence of skin effect, the loss separation principle is still valid, because the three loss items relate to different spatial scales [12]. Thus, by adopting the laminated-Preisach model, Epstein frame measurements are reproduced and energy losses are separated into hysteresis (W_{hyst}), excess (W_{exc}) and eddy current (W_{eddy}) components.

In particular, having computed the time-spatial profile of induced current density $\mathbf{J}(z,t)$ along the lamination thickness, the eddy current losses are estimated as

$$P_{eddy} = \frac{2}{Td}\int_T \int_0^{d/2} \frac{J^2}{\sigma}\, dz dt \qquad (1)$$

being T the period of the time waveform and d the lamination thickness [11]. In absence of minor loops, static hysteresis losses are determined from measurements and linked to the local amplitude of the magnetic flux density. The excess losses are defined as:

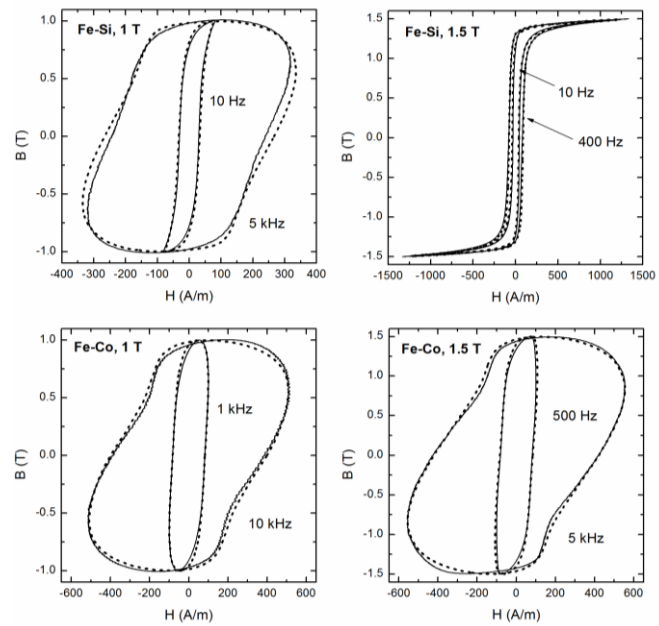

Fig. 2 Dynamic loops measured on Epstein (solid lines) and reconstructed by the laminated-Preisach model (dashed lines) at different frequencies and induction level for the Fe-Si and Fe-Co electrical steels.

TABLE II
MATERIAL PARAMETERS

Parameter	Fe-Si	Fe-Co
Thickness (mm)	0.194	0.201
Elect. Conduct. (S/m)	$1.92\ 10^6$	$2.27\ 10^6$
k_1 ($\text{AT}^{-1}\text{s}^{-1}$)	68	80
k_d ($\text{TmA}^{-1}\text{s}^{-1}$)	563	6340
GV_0S	$5.55\ 10^{-9}$	$5.89\ 10^{-10}$
α	1.675	1.73

$$P_{exc} = \sqrt{\sigma G V_0 S}\,\frac{1}{T}\int_T \left|\dot{B}(t)\right|^{\alpha} dt \qquad (2)$$

where term GV_0S is linked to the k_d constant of DPM. In principle Eqn. (2) is valid only in absence of skin effect with α=1.5. Here, we still adopt this formula, adjusting GV_0S and α in order to fit the results of the laminated-Preisach model. The values obtained by the best fitting are reported in Table II.

The loss separation for the Fe-Co alloy is presented in Fig. 3 and compared with the total measured losses. The curve of the classical losses computed by disregarding skin effect (W_{cl}) is also reported for comparison.

D. Magnetic loss model in the machine

The losses in the stator and rotor cores are computed *a-posteriori*, from the known local time waveforms of the B_x and B_y components of the magnetic flux density. In each mesh element, a magneto-dynamic eddy-current problem is solved using two coupled 1-D diffusion equations where edge effects are disregarded [11]. The resulting components of the current density $\mathbf{J}(z,t)$ along the lamination dept, which include skin effects, are used in (2) to evaluate eddy current losses.

Hysteresis and excess losses are computed as [7]:

$$P_{hyst} = P_{hyst,\max} + P_{hyst,\min}\left[R_{hyst}\left(\hat{B}_{\max}\right)-1\right]$$

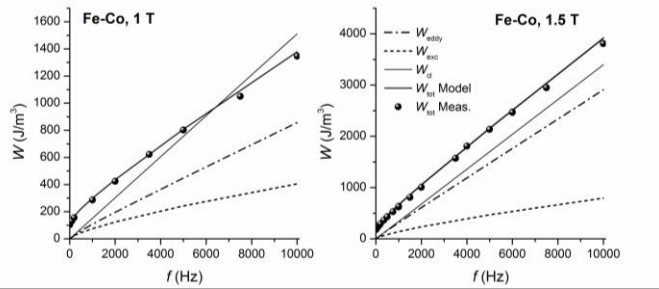

Fig. 3 Loss separation by adopting the laminated-Preisach model for the Fe-Co alloy. The curve of the classical losses (eddy current losses without skin effect), W_{cl} is also reported for comparison.

$$P_{exc} = P_{exc,\max} + P_{exc,\min}\left[R_{exc}\left(\hat{B}_{\max}\right)-1\right]$$

where $P_{hyst,\max}$, $P_{hyst,\min}$, $P_{exc,\max}$, and $P_{exc,\min}$ are the static and the excess power losses (expressed by (2)) calculated along the orthogonal directions defined by the major $B_{\max}$ and minor $B_{\min}$ axes of the local flux density ellipse, respectively. $\hat{B}_{\max}$ is the peak of $B_{\max}$. Functions R_{hyst} and R_{exc} are the experimental defined ratios of pure rotational and pure alternating losses.

IV. Results on the Motogenerator

In the following the results obtained for five different supply frequencies, from 200 Hz to 500 Hz, are presented as multicolumn histograms, to make the comparison of multiple parameters easier.

A. *No-load condition beahavior*

The behavior of iron loss under synchronous no-load conditions is shown in Fig. 4. Up to the 270 Hz, the flux (voltage) linearly increases with the rotational speed (frequency), so that the hysteresis, macroscopic eddy current and excess loss contributions increase following approximately the same behavior found in the Epstein frame material characterization under 1-D flux. Further increasing the frequency, the flux density peak decreases linearly with frequency, since the device is defluxed; in this framework the macroscopic eddy current and excess losses remain almost constant, while the behavior of the hysteresis losses shows a tendency to decrease. The iron losses are mainly concentrated

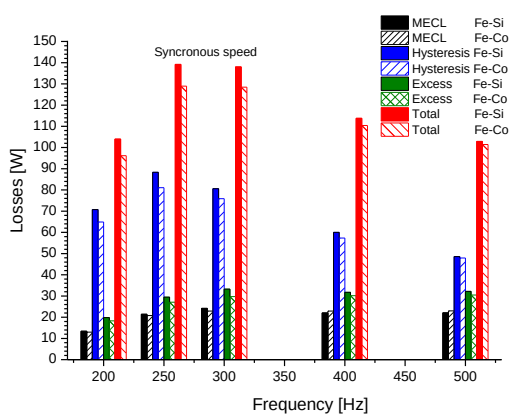

Fig. 4 Computed loss separation at synchronous speed for the machine totally made of silicon iron (Fe-Si) and the one with the rotor in iron cobalt (Fe-Co). Macroscopic eddy current losses are indicated as MECL.

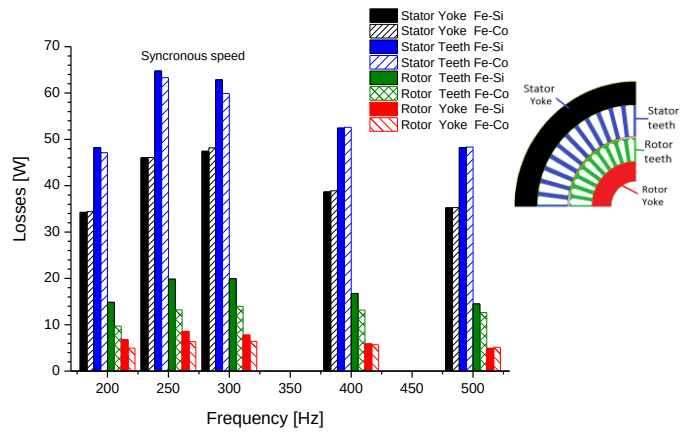

Fig. 5 Distribution of losses within the machine. Four parts (stator yoke, stator teeth, rotor teeth and rotor yoke) are considered.

in the stator, as it can be seen in Fig. 5. The Fe-Co rotor reduces the amount of the rotor losses, especially in the teeth, making the difference between the two materials particularly evident.

B. *Load conditions beahavior*

In the load conditions, both when the machine operates as a motor and when it is acting as a generator (the most interesting working condition), the iron loss significantly increases. This latter, further rises with frequency, as evidenced in Fig. 6, which shows the trend of the total loss in the three following operations: a) motor with 1% slip, b) synchronous no-load conditions, c) generator with 1% slip. Fig. 7 illustrates the distribution of the loss contributions in the three considered operating conditions. One can note that, when deviating from the synchronous speed, both macroscopic eddy current and excess losses rise. Such growth is more pronounced at the frequency increase. The hysteresis loss decreases with frequency and increases significantly passing from the motor operating conditions to the generator ones. In particular, as generator the greatest rise of losses is localized in the stator yoke, and this occurs for both cases, i.e. rotor in Fe-Si and in Fe-Co. There is no room here to show the related histogram.

Table III shows the calculated electrical machine output power for the machine having the Fe-Co rotor. Currents are

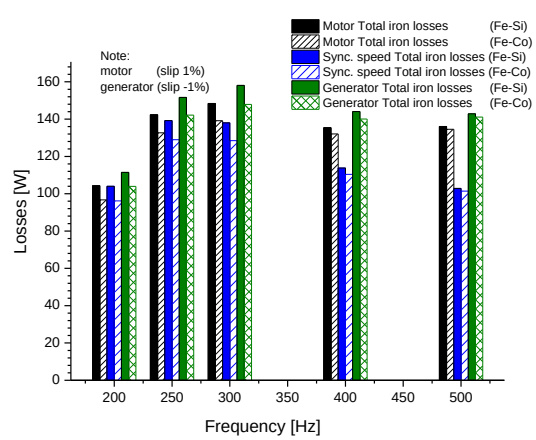

Fig. 6 Comparison among the total amount of iron losses in three different functioning conditions of the motogenerator.

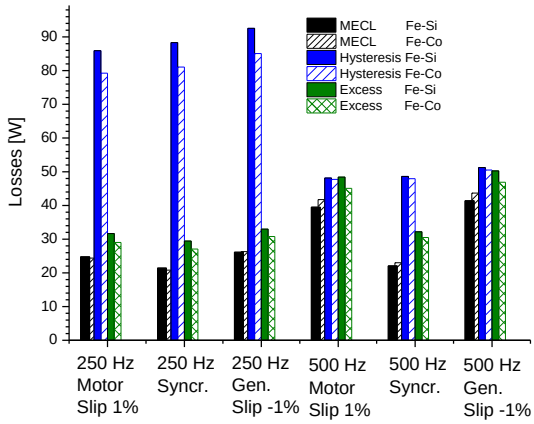

Fig. 7 Comparison of the loss terms among the three operating conditions, at the two frequencies of 250 Hz and 500 Hz, for the machine totally made of iron silicon (Fe-Si) and the one with the rotor made of iron cobalt (Fe-Co). Macroscopic eddy current losses are indicated as MECL.

TABLE III
ELECTRICAL OUTPUT OF THE GENERATOR HAVING THE FE-CO ROTOR

Frequency [Hz]	200	250	300	400	500
Speed [rpm]	6000	7500	9000	12000	15000
Current rms [A]	14.7	17.6	18.2	17.5	17.0
Power [W]	7782	12019	13523	13056	12473
Power [W] (Fe-Si rotor)	7538	11659	13230	13043	12471

average values computed for the 12 phases. Starting from the computation of stator and rotor currents, the Joule losses in the stator windings and rotor bars have been assessed and reported in Fig. 8, together with the electrical machine efficiency. This latter is evaluated neglecting the estimate of the mechanical losses according to

$$\eta = \frac{Pout}{Pout + \sum_{electric+magnetic} losses}$$

It can be noticed that the machine with Fe-Co rotor has a higher output power (3% at 200 Hz, 2% at 300 Hz) with respect to the one adopting a Fe-Si rotor.

V. CONCLUSIONS

For the envisaged application, that is the installation of an electrical machine in the gas turbine of an aircraft, the heating effect is detrimental for the device life and must be reduced and limited. A high speed fault tolerant induction machine seems to be one of the most promising solutions for this challenge. In the studied prototype the iron losses constitute ~12% of the total electric and magnetic losses.

This study demonstrates (Fig. 6) that a reduction of about 7% of the iron losses can be obtained by the use of a rotor made of Fe-Co. This reduction is found in the range 270 Hz - 300 Hz (8-9000 rpm) and reduces at the speed increasing, up to negligible increment at 500 Hz (15000 rpm).

The loss reduction mentioned above corresponds to ~1% of the machine total losses (Fig. 8), which is a significant result, taking into account that the efficiency of the considered device is close to 90%, for all the different regimes.

Moreover, the Fe-Co rotor machine leads to a slightly higher output power (Table III). This paper also provides

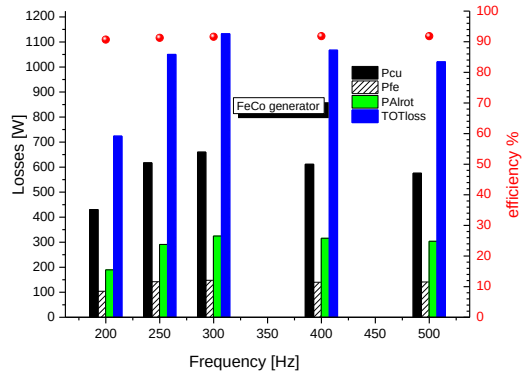

Fig. 8 Machine efficiency and loss terms. Pcu, losses in the winding stator copper, PAlrot, losses in the aluminium bars of the rotor, Pfe, iron losses. Losses are considered in the operating condition of generator for the machine with the rotor made of iron cobalt (Fe-Co). Dots represent the efficiency.

knowledge about loss distribution inside the device and loss separation. Future developments will include the effect on iron losses of different winding configurations and of non-conventional supply conditions.

ACKNOWLEDGMENTS

The here presented results has received funding from the project PRIN 2009 “Advanced characterisation and modelling of magnetic materials for the MEA", financed by MIUR. Many thanks to F. Fiorillo and C. Beatrice who provided the measurements on Fe-Si and Fe-Co laminations.

REFERENCES

[1] M. Hirst, A. McLoughlin, P.J. Norman, S.J. Galloway, “Demonstrating the more electric engine: a step towards the power optimised aircraft”, *IET-Electr. Power Appl.* , Vol. 5, No. 1, pp. 3-13, 2011.

[2] A. Boglietti, A. Cavagnino, A. Tenconi, S. Vaschetto, “The SafetyCritical Electric Machines and Drives in the More Electric Aircraft: a Survey”, Conf. Rec. IEEE- IECON, 2009, pp. 2587-2594.

[3] W. Cao, B. Mecrow, G. Atkinson, J. Bennett, D. Atkinson, “Overview of Electric Motor Technologies Used for More Electric Aircraft (MEA)”, *IEEE Trans. Ind. Electron*., Vol. 59, No. 9, pp. 3523-3531, 2011.

[4] E. Levi, R. Bojoi, F. Profumo, H.A. Toliyat, S. Williamson, “Multiphase induction motor drives – a technology status review*,” IET Electr. Power Appl.*, Vol. 1, No. 4, pp. 489-516, 2007.

[5] A. Tessarolo, C. Bassi, “Stator harmonic currents in VSI-fed synchronous motors with multiple three-phase armature windings,” *IEEE Trans. on Energy Conv*., Vol. 25, No. 4, pp. 974-982, 2010.

[6] F. Scuiller, J.F. Charpentier, E. Semail, “Multi-star multi-phase winding for a high power naval propulsion machine with low ripple torques and high fault tolerant ability,” Proc. of Vehicle Power and Propulsion Conference, pp. 1-5, 1-3 Sept. 2010, Lille, France.

[7] O. Bottauscio, M. Chiampi, A. Manzin, M. Zucca, "Additional Losses in Induction Machines under Synchronous No-Load Conditions", IEEE Trans. Magn., Vol. 40, No. 5, 2004, pp. 3254-3261.

[8] O. Bottauscio, M. Chiampi, M. Zucca, "Experimental and numerical investigations on rotational fluxes in stator cores of three-phase motors", *IEEE Trans. Magn*., Vol. 38, No. 5, pp. 3294-3296, 2002.

[9] P. Sergeant, F. De Belie; L. Dupre, et al., “Losses in Sensorless Controlled Permanent-Magnet Synchronous Machines” *IEEE Trans. Magn.*, Vol. 46, No 2, pp 590-593, 2010.

[10] P. Rasilo, A. Belahcen, A. Arkkio, “Importance of Iron-Loss Modeling in Simulation of Wound-Field Synchronous Machines”, *IEEE Trans. Magn.*, Vol. 48, No 9 pp. 2495-2504, 2012.

[11] O. Bottauscio, M. Chiampi, "Laminated core modelling under rotational excitations including eddy currents and hysteresis", *Journal of Applied Physics*, Vol. 89, No. 11, pp. 6728-6730, 2001.

[12] G. Bertotti, Hysteresis in Magnetism: For Physicists, Materials Scientists, and Engineers, San Diego, Academic Press, 1998